LETTER

$\mathcal{PT}$ symmetric sonic crystals: From asymmetric echoes to supersonic speeds

A Letters Journal Exploring the Frontiers of Physics

November 2018

EPL, **124** (2018) 34001
doi: 10.1209/0295-5075/124/34001

www.epljournal.org

$\mathcal{PT}$ symmetric sonic crystals: From asymmetric echoes to supersonic speeds

M. Rosendo-López, A. Merkel and J. Christensen[(a)]

Department of Physics, Universidad Carlos III de Madrid - Avenida de la Universidad, 28911 Leganés (Madrid), Spain

received 3 September 2018; accepted in final form 26 October 2018
published online 27 November 2018

PACS 42.82.-Et – Waveguides, couplers, and arrays

Abstract – Parity-time $\mathcal{PT}$ symmetric structures based on balanced distributions of gain and loss have attracted significant attention in acoustic metamaterial research since they allow one to sculpture the flow of sound waves in complete new ways. We compute complex Bloch waves in fluidic non-Hermitian sonic crystals and demonstrate how band coalescence can lead to exceptionally large group velocities permitting supersonic wave propagation in $\mathcal{PT}$ symmetric slabs. Further, by controlling the degree of non-hermiticity in such systems, we found that asymmetrically reflected pulses can be readily amplitude-tuned, which might find potential use in echocardiography, sonar and echo suppressors.

Modulating in space at least two distinct media leads to unexpected wave propagation properties. Based on diffraction and local resonances, exciting phenomena are born in artificial media when the modulation takes place in phononic and sonic crystals, but also when it occurs at subwavelength scale [1]. The modulation conventionally concerns only the real part of the material parameters, but the modulation of the imaginary counterpart can also give rise to rich physics and intriguing effects. Particularly, when media variations are realized via the imaginary parts of the material parameters, *i.e.*, a modulation of gain and loss, then one is able to explore the physical features that are consequences of the parity-time $\mathcal{PT}$ symmetry of the system.

$\mathcal{PT}$ symmetry describes the invariance of a non-Hermitian system that despite complex entities can still have real eigenvalue spectra. In such system, two operators are employed, namely the parity $\mathcal{P}$ operator, which accounts for the inversion of the space coordinates and the time-reversal $\mathcal{T}$ operator, which reverses the sign of the time parameter [2]. $\mathcal{PT}$ symmetry usually requires a careful balance of gain and loss in the physical systems. Systems obeying $\mathcal{PT}$ symmetry have been extensively studied in many areas of wave physics, including optics and acoustics. A host of interesting acoustical phenomena have been studied, including unidirectional invisibility, constant acoustic pressure in non-Hermitian disordered media, wave vector manipulation in two dimensions and the valley-Hall effect in non-Hermitian artificial acoustic boron nitride [3–8].

In order to realize the parameters in a practical structure one has to utilize media with an appropriate complex behaviour in terms of both loss and gain. Loss, or sound attenuation, obviously is the least challenging material parameter to obtain as a broad range of porous media or resonators can give the desired response. Acoustic gain, on the other hand, is a less conventional response and requires special "activations" in order to amplify sound waves. In order to realize this, and to provide the exact time-reversed image of gain, that is, the loss counterpart, in the literature one currently finds few ways to do so. For one, a pair of loudspeakers loaded with suitably tailored non-Foster electrical circuits can be employed that, in principle, can provide a broad variety of $\mathcal{PT}$ symmetric conditions [4]. By the use of the electro-acoustic effect in electrically biased piezoelectric semiconductors the imaginary part of the stiffness modulus can be tuned and altered via the electric field, carrier concentration, and frequency [9,10]. It was shown that sound waves in an airflow duct going through a pair of diaphragms, with equivalent amounts of flow-induced gain and loss, display $\mathcal{PT}$ symmetry [11]. Similar to [4], but for elastic waves, loss and gain have been achieved in piezoelectric ceramics when shunted by external circuits containing positive

[(a)]E-mail: johan.christensen@uc3m.es (corresponding author)

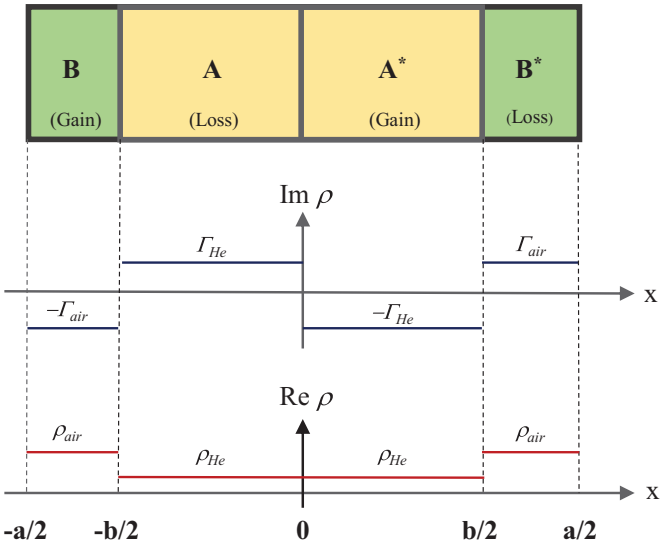

Fig. 1: (Color online) Schematic of the unit cell of the $\mathcal{PT}$ symmetric sonic crystal composed of air and helium fluid layers. In order to fulfil the $\mathcal{PT}$ symmetry condition we design a non-Hermitian crystal where the real part of $\rho(x)$ is an even function in space but its imaginary counterpart is an odd one. The total length of the considered unit cell is $a = 1$ cm and $b = 0.8a$.

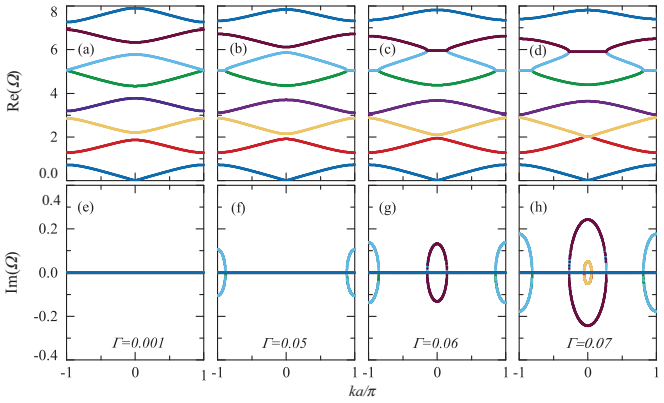

Fig. 2: (Color online) Evolution of the complex band diagram of the $\mathcal{PT}$ symmetric sonic crystal as a function of the non-hermiticity parameter Γ. The top panels (a)–(d) show the real parts of the Bloch eigenfrequencies and the bottom panels (e)–(h) display their imaginary parts. The various non-hermiticity parameters employed are given in their respective sub-panels.

and negative resistances [12]. Thus, it can be concluded that one is able to obtain any desired acoustic response in active acoustic metamaterials.

Whereas $\mathcal{PT}$ symmetry has been extensively studied in photonics [5,13,14], the effects of $\mathcal{PT}$ symmetry in periodic acoustic structures have been less investigated. In this letter, we numerically investigate a non-Hermitian one-dimensional sonic crystal (SC) where complex band diagrams are computed in dependence of the non-hermiticity parameter that determines the amount of loss and gain. The complex acoustic band diagrams exhibit mode coalescences, and various exceptional points (EPs) beyond which, acoustic Bloch states are allowed to either amplify or attenuate sound within the $\mathcal{PT}$ broken phase. The mode coalescence displays steep band degenerations with exceptional high group velocity permitting the launching of supersonic transient pulses. Furthermore, we also predict how unidirectional zero reflection (UZR) in the vicinity of the EPs extends to highly asymmetric reflected pulses. Deterministically controlling acoustic echoes and producing supersonic pulse propagation in $\mathcal{PT}$ symmetric crystals provide new routes in designing novel waveguides and couplers in phononic circuits.

We stated earlier that, based on active acoustic metamaterials, one is able to mimic any desired acoustic response. Henceforth, we embark on the study by employing an entirely fluidic crystal whose complex response is assumed to be controlled by, *e.g.*, externally applied electronic circuits to account for lossy or amplifying acoustic wave propagation. Along this front we thus employ typical fluids whose imaginary terms of the mass density can be varied as desired. The one-dimensional SC is composed of an air layer with bulk modulus $K_{\mathrm{air}} = 1.44 \cdot 10^5\,\mathrm{kg/ms^2}$, mass density $\rho_{\mathrm{air}} = 1.225\,\mathrm{kg/m^3}$ and speed of sound $c_{\mathrm{air}} = 343.2\,\mathrm{m/s}$, and a helium layer with $K_{\mathrm{He}} = 1.50 \cdot 10^5\,\mathrm{kg/ms^2}$, $\rho_{\mathrm{He}} = 0.175\,\mathrm{kg/m^3}$ and $c_{\mathrm{He}} = 927\,\mathrm{m/s}$, as shown in fig. 1. In order to meet the $\mathcal{PT}$ symmetry condition, the complex mass densities of the layered unit cell must satisfy $\rho(x) = \rho^*(-x)$, while, here, the bulk moduli are kept real, *i.e.*, $K(x) = K(-x)$ [3]. To this end, we introduce an imaginary part to the mass densities via a non-hermiticity parameter $\Gamma_{\mathrm{air}} = \Gamma_{\mathrm{He}} \equiv \Gamma$ such that the complex densities obtain $\rho_{\mathrm{air,He}} = \rho_0(1 \pm i\Gamma)$, where ρ_0 refers to the respective conventional mass density and the plus and minus signs represent loss and gain, respectively.

The complex band structure is obtained by employing the plane-wave expansion method [15] where the wave number k is held real and, as a consequence, the Bloch eigenfrequencies $\Omega = \omega a/(2\pi c_{\mathrm{air}})$ can be complex. As shown in fig. 2, we compute the complex band diagrams for various values of the non-hermiticity parameter Γ. Beginning with a relatively small amount of loss and gain, *i.e.*, $\Gamma = 0.001$, the spectrum of Bloch eigenmodes remains purely real, as can be seen in fig. 2(a) and (e). As the non-hermiticity parameter Γ increases, the real part of the eigenfrequencies of some of the Bloch eigenmodes coalesce either at the edge or at the center of the Brillouin zone, making the width of the band gap shrink as can be seen in fig. 2(a)–(d). The corresponding imaginary parts of the coalesced Bloch eigenmodes are complex conjugate, as shown in fig. 2(f)–(h), indicating the emergence of a $\mathcal{PT}$-broken phase in the k-space. In the absence of mode coalescence, all eigenfrequencies remain purely real, indicating the occurence of an exact $\mathcal{PT}$ symmetric phase in the k-space. The EPs marking the onset of this phase

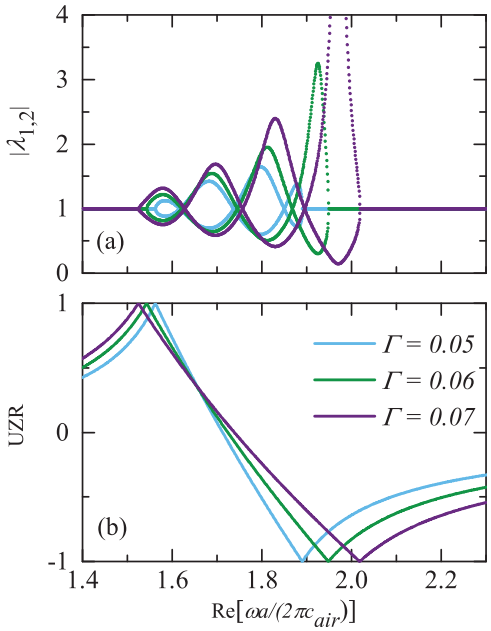

Fig. 3: (Color online) Computed eigenvalues and *UZR* for different values of the non-hermiticity parameter Γ. (a) Modulus of the eigenvalues $\lambda_{1,2}$ of the scattering matrix. (b) Unidirectional zero reflection coefficients.

transition always appear in pairs due to intact time symmetry. Again we stress that all simulations have been performed for the case with filling fraction $f = \frac{b}{a} = 0.8$. Changing the filling fraction would result in variations of the dispersion relation and consequently in spectral shifts of the EPs.

In order to study the complex scattering properties in finite SCs we employ the transfer matrix method (TMM) with the scattering matrix

$$S = \begin{pmatrix} t & r_R \\ r_L & t \end{pmatrix}, \tag{1}$$

where t is the complex and reciprocal transmission coefficient, $r_{L,R}$ are the complex reflection coefficients from the left L and right R, respectively. The transmittance T is defined as $T = |t|^2$, the reflectances from the left L and right R are defined as $R_{R,L} = |r_{L,R}|^2$, respectively. The $\mathcal{PT}$ condition for the scattering matrix is $r_L r_R^* = r_L^* r_R = 1 - |t|^2$ and the $\mathcal{PT}$-exact (-broken) phase, where the eigenvalues of the scattering matrix $\lambda_{1,2}$ are (not) unimodular, happens for $T < 1$ ($T > 1$). An EP of the scattering matrix S forms when $T = 1$, when either $R_L = 0$ or $R_R = 0$ and $R_L \neq R_R$ [16]. To quantifiy spectrally the onset of the reflectance asymmetries we study the unidirectional zero reflection (*UZR*) coefficient that is defined as $UZR = (R_L - R_R)/(R_L + R_R)$. The *UZR* coefficient is equal to 1 (−1) when the right (left) reflectance vanishes [17]. When comparing the *UZR* coefficient with the eigenvalues of the scattering matrix for three different values of the non-hermiticity parameters in a finite SC with $N = 7$ cells, one can see in fig. 3 that not all the eigenvalue transitions from unimodular to non-unimodular correspond to $UZR = \pm 1$. It is however the onset of this transition that defines the spectral location where the reflectance vanishes for one-sided irradiation. This onset can be spectrally shifted by increasing Γ. Surrounding the spectral point beyond which the symmetry of the reflectances breaks ($R_L = R_R$, *i.e.*, $UZR = 0$), several Bragg resonances that scale with the number of unit cells appear in the form of unimodular phase oscillations as seen in the plot of $|\lambda_{1,2}|$ in fig. 3(a). As mentioned before however, $UZR = \pm 1$ only takes place at the EPs where non-oscillatory eigenvalues coalesce [18].

In what follows, we present a more comprehensive study where the reflectances are computed in dependence of the frequency and the non-hermiticity parameter. In doing this, we choose two cases of given layer thickness. For the simplest case when $N = 1$, the contours of the zero reflectances from either left or right insonification in the Ω-Γ parameter plane correspond to the contours of $UZR = \pm 1$ as can be seen in fig. 4(a)–(c). These zeros are associated with a unity transmittance $T_1 = 1$ following the property of the EP. When extending the tickness to $N = 7$, the zero reflectances associated with Bragg resonances appear in addition, however, *UZR* linked to the EPs remain unchanged as shown in fig. 4(d)–(f). The transmittance T_N of a finite SC with N cells emerges from the transmittance of a single unit cell T_1 [19–21],

$$\frac{1}{T_N} = 1 + \left(\frac{1}{T_1} - 1\right)\frac{\sin^2(N\phi)}{\sin^2\phi}, \tag{2}$$

where ϕ is the Bloch phase. Equation (2) is valid both for Hermitian and $\mathcal{PT}$ symmetric systems. Irrespective of the number of unit cells the *UZR* contours from fig. 4(a) and fig. 4(d) remain identical. We can explain this by the unity transmittance in a single unit cell $T_1 = 1$ at the EP. When this condition is met, a structure composed of N cells necessarily must always sustain full transmittance $T_N = 1$ as found in eq. (2).

Interestingly, what fig. 4 further reveals is the ability also to control the amplitude of the reflected waves through the non-hermiticity parameter, which differs substantially with the side of the sample onto which sound is insonified. To study this property in view of real-world spectroscopical applications and broadband signal processing we proceed with the investigation using time-domain predictions of scattered pulses. Thus, to be able to control reflected pulses from non-Hermitian layered media is highly useful for echo suppression and signal manipulation in echocardiography and sonar. We consider an incident pulse $f(t)$, which is a cosine function modulated by a Gaussian envelope and is written as $f(t) = \cos(\omega_0 t)e^{-t^2/(2\sigma_f)^2}$, where ω_0 is the central frequency of the pulse and $1/\sigma_f$ is the frequency half-width. The scattered pulses are obtained by inverse Fourier transformation of the product of the corresponding scattering coefficient with the Fourier spectrum of the incident pulse [22]. In order to keep the width of the pulses narrow

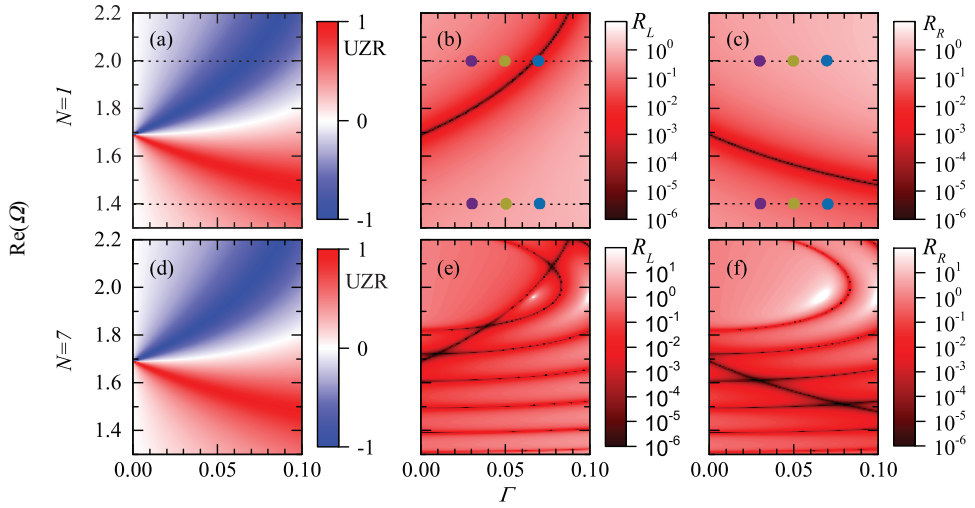

Fig. 4: (Color online) Dependence of the reflectances in finite size SCs, composed of (a)–(c) one unit cell and (d)–(f) seven unit cells, at various non-hermiticity parameters Γ. (a) and (d): *UZR* coefficients; (b) and (e): R_L; and (c) and (f): R_R as a function of Re(Ω) and Γ. The colored dots in (b) and (c) correspond to the examples computed in in fig. 5.

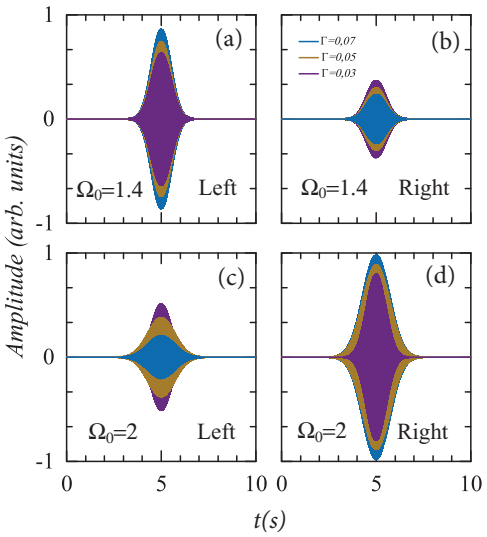

Fig. 5: (Color online) Reflected pulses from a finite SC centered in time at 5 s, from the left ((a), (c)) and from the right side ((b), (d)) for various non-hermiticity parameters Γ. The central frequency of the Gaussian pulse in (a), (b) is $\Omega_0 = 1.4$ and in (c), (d) $\Omega_0 = 2$.

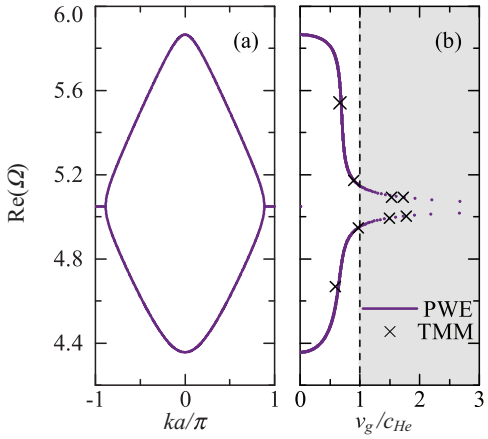

Fig. 6: (Color online) Group velocity for the fifth and the sixth modes of the periodic SC for $\Gamma = 0.05$. (a) Real part of the dispersion relation. (b) Group velocity predicted from the band diagram of the periodic SC (dots) and from the time-domain analysis of a finite SC (crosses).

in frequency, the width in time is chosen to be $\sigma = 0.5$ s. For simplicity, we focus initially on the simplest configuration, *i.e.*, $N = 1$ and concentrate on the marked locations of the Ω-Γ contours in fig. 4(b) and fig. 4(c). The spectral cuts across the contours correspond to suppressed echoes from the right at a central frequency $\Omega_0 = 1.4$ and similarly from the left, provided that $\Omega_0 = 2.0$, which is computed in fig. 5. When the non-hermiticity parameter slowly is increased as indicated, the amplitude of the reflected pulse from the left (right) increases, whereas the reflected pulse from the right (left) decreases since we approach the EP as depicted in fig. 5 at $\Omega_0 = 1.4$ (2.0). Thus, the non-hermiticity parameter Γ can act as an amplitude modulator of reflected pulses, by attenuating them from one side while, at the same time, amplifying the signals from the opposite side of the slab.

What appeared to be highly unusual in the complex band diagrams discussed in fig. 2, is the pronounced steepness of the coalesced branches near the EPs suggesting supersonic group velocities as has been suggested elsewhere for the case of light [23]. As opposed to the previous discussion on tunable echoes, we now aim at transmitting supersonic signals through finite non-Hermitian crystals. In the nearest vicinity of the EPs, the $\mathcal{PT}$ symmetry phase transition is accompanied by branch splitting that have exceptionally large group velocities $v_g = \partial\omega/\partial k$ as seen in fig. 6(a). This group velocity in the periodic scenario has been computed for the fifth and sixth band in fig. 6(b) in which it is clearly shown how supersonic speeds

($v_g > c_{He}$) have been reached when approaching the EP. We compare the speed of sound of a transmitted acoustic pulse traversing a finite SC of $N = 30$ cells by finding the pulse delay time τ_d via the arrival time of 10% of the maximum Gaussian envelope. The group velocity is then determined by $v_g = Na/\tau_d$ and compared to the periodic case as shown in fig. 6(b). There is a good agreement between the periodic and finite computation of v_g suggesting that coalesced steep branches in non-Hermitian crystals can lead to supersonic wave transmissions.

In summary, we have studied periodic and finite one-dimensional non-Hermitian sonic crystals and found new ways to design unusual wave propagation in dependence on the balanced gain and loss strength. Beyond the coalescence of complex Bloch modes, we have conducted in-depth transient analysis and found that asymmetrically reflected pulses can be readily tuned by means of the non-hermiticity parameter and we discussed how one is able to engineer supersonic group velocities in the vicinity of an exceptional point hosting almost entirely vertical dispersion bands. We foresee that our findings can advance sonar and echo control applications in the non-destructive community and in medicine.

* * *

JC acknowledges the support from the European Research Council (ERC) through the Starting Grant No. 714577 PHONOMETA and from the MINECO through a Ramón y Cajal grant (Grant No. RYC-2015-17156). Also fruitful comments from Daniel Torrent and Romain Fleury are appreciated.

REFERENCES

[1] Cummer S. A., Christensen J. and Alu A., *Nat. Rev. Mater.*, **1** (2016) 16001.
[2] Bender C. M. and Boettcher S., *Phys. Rev. Lett.*, **80** (1998) 5243.
[3] Zhu X., Ramenazi H., Shi C., Zhu J. and Zhang X., *Phys. Rev. X*, **4** (2014) 031042.
[4] Fleury R., Sounas D. and Alù A., *Nat. Commun.*, **6** (2015) 5905.
[5] El-Ganainy R., Makris K. G., Khajavikhan M., Musslimani Z. H., Rotter S. and Christodoulides D. N., *Nat. Phys.*, **14** (2018) 11.
[6] Rivet E., Brandstötter A., Makris K. G., Lissek H., Rotter S. and Fleury R., *Nat. Phys.*, **14** (2018) 942.
[7] Liu T., Zhu X., Liang F. C. S. and Zhu J., *Phys. Rev. Lett.*, **120** (2018) 124502.
[8] Wang M., Ye L., Christensen J. and Liu Z., *Phys. Rev. Lett.*, **120** (2018) 246601.
[9] Christensen J., Willatzen M., Velasco V. R. and Lu M.-H., *Phys. Rev. Lett.*, **116** (2016) 207601.
[10] Christensen J., *EPL*, **114** (2016) 47007.
[11] Aurégan Y. and Pagneux V., *Phys. Rev. Lett.*, **118** (2017) 174301.
[12] Hou Zhilin and Assouar B., *J. Appl. Phys.*, **123** (2018) 085101.
[13] Regensburger A., Bersch C., Miri M.-A., Onishchukov G., Christodoulides D. N. and Peschel U., *Nature*, **488** (2012) 167.
[14] Ding K., Zhang Z. Q. and Chan C. T., *Phys. Rev. B*, **92** (2015) 235310.
[15] Kittel C., *Introduction to Solids State Physics* (John Wiley and Sons, New York) 1966.
[16] Ge L., Chong Y. D. and Stone A. D., *Phys. Rev. A*, **85** (2012) 023802.
[17] Zhu X.-F., Peng Y.-G. and Zhao D.-G., *Opt. Express*, **22** (2014) 18401.
[18] Shramovka O. V. and Tsironis G. P., *J. Opt.*, **18** (2016) 105101.
[19] Sprung D. W. L., Wu H. and Martorell J., *Am. J. Phys.*, **61** (1993) 1118.
[20] Bendickson J. M., Dowling J. P. and Scalora M., *Phys. Rev. E*, **53** (1996) 4107.
[21] Alaee R., Christensen J. and Kadic M., *Phys. Rev. Appl.*, **9** (2018) 014007.
[22] Merkel A., Willatzen M. and Christensen J., *Phys. Rev. Appl.*, **9** (2018) 034033.
[23] Szameit A., Rechtsman M. C., Bahat-Treidel O. and Segev M., *Phys. Rev. A*, **84** (2011) 021806.